J Appl Electrochem (2008) 38:1561–1569
DOI 10.1007/s10800-008-9598-z

ORIGINAL PAPER

Electrodeposition of Cu from acidic sulphate solutions containing cetyltrimethylammonium bromide (CTAB)

Benedetto Bozzini · Lucia D'Urzo · Marilena Re · Federica De Riccardis

Received: 28 December 2007 / Accepted: 16 May 2008 / Published online: 28 May 2008

Abstract In this paper we report a study of the electrodeposition of Cu from an acidic sulphate solution containing cetyltrimethylammonium bromide (CTAB). This investigation is based on cyclic voltammetry, in situ surface-enhanced Raman spectroscopy (SERS), Scanning Electron Microscopy (SEM) and Transmission Electron Microscopy (TEM). Adsorption of CTAB over a wide range of cathodic potentials was proved spectroelectrochemically, encompassing both conditions where compact and loose Cu grows (up to −0.4 and between −0.4 and −1 V vs. Ag/AgCl, respectively). Furthermore, we found that CTAB tends to react cathodically, undergoing the loss of the aliphatic tail at lower cathodic potentials and the formation of an allylic product at higher polarisations. CTAB deeply impacts the Cu growth mode: ordered ridges of compact Cu crystallites form at low cathodic potentials—where the electrodeposition process is strongly inhibited by CTAB adsorption—and nanoparticles grow under hydrogen-evolution conditions.

Keywords Electrodeposition · Copper · Nanoparticles · CTAB · SERS

B. Bozzini (✉) · L. D'Urzo
Dipartimento di Ingegneria dell'Innovazione,
Università di Lecce, via Monteroni,
73100 Lecce, Italy
e-mail: benedetto.bozzini@unile.it

M. Re · F. De Riccardis
ENEA—Materials and Technology, Composite and
Nanostructured Materials Section, C.R. Brindisi,
S.S. 7 Appia – km 706, 72100 Brindisi, Italy

1 Introduction

The use of quaternary ammonium salts (QAS), extensively reported in the electroplating (ECP) literature as inhibitor or catalyst [1–9] is currently receiving renewed attention due to the possibility of their use as templating agents and nanoparticle coaters.

The special interfacial chemistry of some QASs, such as CTAB—leading to a rich concentration-dependent phase scenario (see e.g. [10])—lends itself to the formation of ordered two- and three-dimensional organic, electrically insulating structures at the electrode–electrolyte interface, that selectively mask parts of the electrode and offer ionic conducting paths that provide ideal templating characteristics that may lead to the achievement of unprecedented shaping capability and lateral resolution in the growth of metals, as well as other materials that can be grown by electrodeposition (e.g. [11] and references therein).

Furthermore, ECP is one of the processes viable for nanoparticle fabrication, although the colloidal route has received more attention. In particular, ECP in the presence of quaternary ammonium salts (QAS), such as $(C_8H_{17})_4NBr$, has been practised as a way of preparing mono- and bimetallic nanoparticles (1–10 nm in diameter) in the form of colloidal precipitates. The following systems have been reported: Ag, Au, Co, Fe, Mo, Ni, Pd, Pt, Rh, Ru, Fe–Co, Fe–Ni, Pd–Cu, Pd–Ni, Pd–Pt, Pt–Ru, Pt–Sn [12–18]. These "nano-plating" processes rely on: (A) ECP from electrolytes with extremely low metal cation concentrations, typically achieved by using a metal-free electrolyte and soluble anodes; (B) ready precipitation of the colloids. The cathodic reaction can be schematically described as:

$$M^{z+} + ze^- + QAS \rightarrow M_{colloid}/QAS \downarrow$$

The preparation of double layer Pt/Pd nanoparticles has also been reported, with a Pt core of 3.8 nm and an overall diameter of 5 nm [16]. The synthetic process consists in electrolysing a solution containing Pt colloids protected by $(C_8H_{17})_4NBr$ in the presence of excess QAS with a Pd soluble anode. The electrochemical approach to the synthesis of metallic nanoparticles has been claimed to exhibit size-selectivity capability and a high degree of monodispersity, chiefly controlled by c.d., with cell geometry, electrolysis time, T and nature of the solvent as concomitant factors.

In the present paper we report an investigation on the ECP of Cu nanoparticles from an acidic sulphate solution containing CTAB above the critical micellar concentration (CMC) [19]. This investigation is based on cyclic voltammetry (CV), in situ SERS, SEM and TEM. The aim of this work is to elucidate the interfacial chemistry of the QAS in view of achieving a more insightful understanding of the metal-structuring activity of organics adsorbed at the growing cathode chiefly in terms of metallic nanocrystal production.

2 Experimental

The basic ECP bath was of the type commonly used for interconnect fabrication in ULSI applications (for details, see, e.g. [20] and references therein): $CuSO_4{\cdot}5H_2O$ 20 mM, H_2SO_4 0.5 M, NaCl 10 mM. To this electrolyte, 0.5 and 2.5 mM cetylammonium bromide (CTAB) was added. These concentrations are below and above the CMC of CTAB in the relevant electrolyte as measured by us with the Wilhelmy balance method (0.72 ± 0.11 mM in ultra-pure water, 1.93 ± 0.38 mM in the Cu plating solution). The solutions were prepared from analytical grade chemicals and ultra-pure water with a resistivity of 18.2 MΩ cm. The solutions were degassed by bubbling with Ar during the measurements. Oxygen-free high-purity polycrystalline Cu rods were used as electrodes. Before each experiment the Cu substrate was electropolished in 65 vol% H_3PO_3 with a cell potential of 2 V and a Pt foil counterelectrode.

Electrochemical measurements were performed with an AMEL 5000 programmable potentiostat. Potential measurements were carried out with an AMEL Ag/AgCl reference electrode containing a 3 M KCl separated from the electroplating solution by a porous ceramic insert. Potentials are reported vs. Ag/AgCl.

SERS measurements were performed with a LabRam confocal Raman system. Excitation at 633 nm was provided by a He-Ne laser, delivering 7 mW at the sample surface. A 50 × long-working-distance objective was used. In situ spectroelectrochemistry was carried out in a cell with a vertical polycrystalline Cu disc working-electrode (WE) of diameter 5 mm embedded in a Teflon cylindrical holder. A metallographic polishing procedure, consisting of wet grinding with 2400 grit SiC paper, allowed excellent reproducibility. The counter-electrode was a Pt wire loop (1.25 cm^2) concentric and coplanar with the WE disc. The reference electrode (RE) was placed in a separate compartment. The RE probe tip was placed 3 mm from the rim of the working electrode disc. Raman intensities are normalised over the acquisition time—so that the intensities can be compared—and proportional to the discharge current of the CCD element corresponding to a given Raman shift, uncorrected for quantum efficiency.

SEM observations were carried out with a Cambridge Stereoscan 360 SEM. The electron source was LaB_6, the electron detection was carried out with a scintillation photodetector.

For TEM observations, we employed a TECNAI G^2 F30 microscope, operated with an acceleration voltage of 300 kV and with a point resolution of 0.205 nm. In particular conventional Bright Field (BF) images and High-Resolution Transmission Electron Microscope (HRTEM) images were obtained for all the samples, which were prepared for TEM observations by depositing on Carbon coated Cu grids some droplets of powders dispersed in the plating bath to which an excess of $NaSO_3$ and CTAB were added after plating, as chemical stabilisers.

Surface tension measurements were carried out with a NIMA Technology surface pressure sensor type PS4.

3 Results and discussion

3.1 Cyclic voltammetry experiments

3.1.1 ECP bath without CTAB

CVs measured in the potential ranges −0.5 to 0.75 V and −0.75 to 0.75 V for the ECP bath in the absence and presence of Cl^- are shown in Fig. 1. The formation of Cl^--complexes has the following effects: (i) the nucleation potential (as evaluated from the current-crossover η_{co}) becomes ennobled by ca. 75 mV; (ii) the equilibrium potential (again, as evaluated from η_{co}) is denobled by ca. 25 mV; (iii) the stripping peak is denobled. The complex chemistry of aqueous solutions containing Cu^+, Cu^{2+} and Cl^- (e.g. [21]) correlates with the presence of multiple peaks in the stripping curve. Two well-defined peaks are seen: (i) the more cathodic one—corresponding to the oxidation of metallic Cu to Cu^+ [22, 23]—exhibits three components (A-I, A-II and A-III), related to the formation of sparingly soluble Cu(I) chloro-complexes; (ii) the more anodic one (B) is due to the oxidation of Cu(I) to Cu(II) and is controlled by both the stability of Cu(I) chlorocomplexes and mass transport.

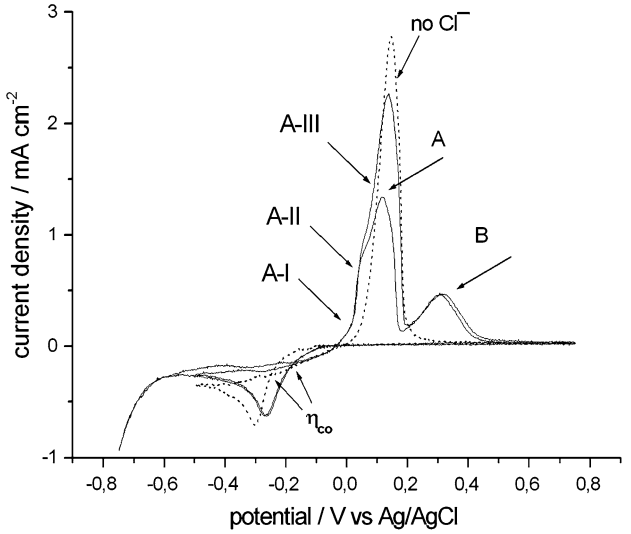

Fig. 1 Cyclic voltammetry for Cu electrodeposition from the solution containing 0.5 mM CTAB. Scan rate: 20 mV s^{-1}. Labels A-I, A-II, A-III, A and B refer to the mechanistic discussion contained in the main text

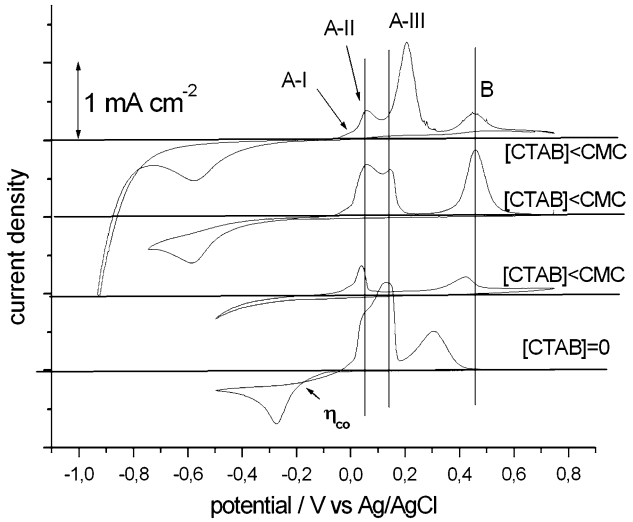

Fig. 2 Cyclic voltammetry for Cu electrodeposition from the solution containing 0.5 mM CTAB. Scan rate: 20 mV s^{-1}, different cathodic terminal voltages. Labels A-I, A-II, A-III and B refer to the mechanistic discussion contained in the main text

On decreasing the cathodic terminal voltage (CTV) from −0.5 to −0.75 V the cathodic features and peaks A-I, A-II and B are essentially unaffected; therefore the progressive growth of ECP metal seems to affect just feature A-III, that can thus be related to readily soluble species, while features A-I and A-II may correspond to surface layers of low nobility and A-III to a pseudopassivating saturated layer. Layers of this kind are very often formed when porous, insoluble corrosion-product films form at metal electrodes (e.g. [24]). Replicate runs measured in the interval 0.75/− 0.5 V after having performed the experiments with CTV −0.75 mV exhibit no hysteresis.

3.1.2 ECP bath with 0.5 mM CTAB

The experiments described in this Section were performed with a CTAB concentration lower than the CMC (ca. 2 mM). CVs measured after injection of CTAB to 0.5 mM with different CTVs are reported in Fig. 2. Addition of the QAS gives rise to the following voltammetric changes.

(i) The cathodic c.d. in the return scan is lower than in the forward one. Furthermore, no current-crossover points η_{co} are found; this fact can be interpreted in terms of nucleation inhibition caused by cathodic adsorption. This type of inhibition can be rationalised in terms of adsorbed Cu(I) chlorocomplexes, as commented in Sect. 3.1.1.

(ii) The equilibrium potential shifts cathodically by ca. 40 mV. Owing to the absence of a c.d. crossover point η_{co} in the experiments carried out in the presence of CTAB, we estimate the equilibrium potential by identifying it with the potential at which the return scan crosses the zero c.d. line.

(iii) The ECP potential is shifted cathodically, in particular the voltammetric peak is denobled by ca. 315 mV.

(iv) As far as the anodic stripping peak is concerned, the following is seen: (a) for CTVs −0.5 and −0.75 V the complex peak A is found essentially in the same potential ranges both in the absence and presence of CTAB. Nevertheless, the relative intensities of the components I, II and III are a function of the CTV; (b) with a CTV of −0.1 V peak A-III shifts anodically by ca. 70 mV. It is worth noting that, in the presence of 0.5 mM CTAB, the CVs do not change appreciably upon scanning the potential for over 30 cycles in the ranges 0.75 to −0.5 V and 0.75 to −0.75 V; (c) peak B shifts anodically by ca. 160 mV, such a shift denotes a protective action of the organic on the pseudopassive layer.

3.1.3 ECP bath with 2.5 mM CTAB

CVs measured after injection of CTAB to 2.5 mM, a final concentration higher than the CMC (ca. 2 mM), together with a CV from the additive-free bath, for comparison, are reported in Fig. 3. The corresponding CVs measured in the presence of 0.5 mM CTAB are also shown for comparison. In Fig. 3 the qualitative voltammetric features are not changed upon increasing the CTAB concentration above the CMC; some quantitative aspects can be noticed: (i) lower c.d.s, compatible with a higher electrode coverage

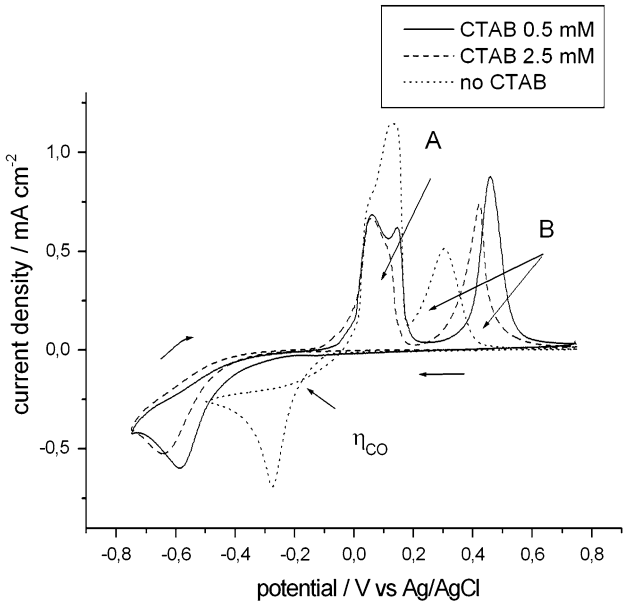

Fig. 3 Cyclic voltammetry for Cu electrodeposition from solution containing: 0, 0.5 and 2.5 mM CTAB. Scan rate: 20 V s^{-1}. Labels A and B refer to the mechanistic discussion contained in the main text

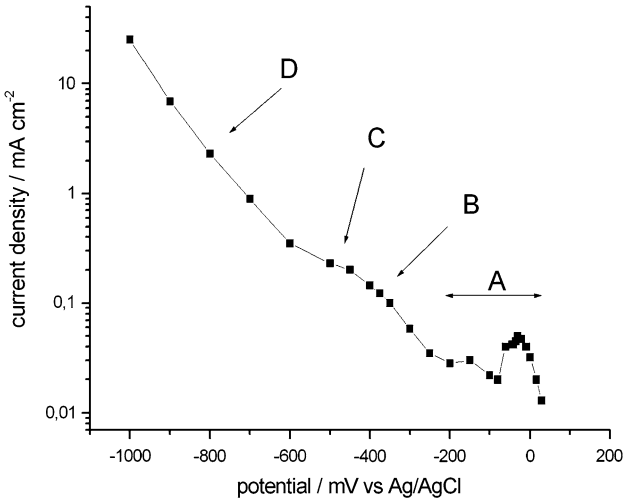

Fig. 4 Steady-state potential-c.d. curve, recorded during SERS measurements, for Cu electrodeposition from solution containing 2.5 mM CTAB. Labels A, B, C and D refer to the mechanistic discussion contained in the main text

with the organic, (ii) denobling of peak A, (iii) a variation of the relative intensities of peaks A and B, as well as of the components of peak A. The presence of micellae in the solution thus does not bring about any specific qualitative changes in the CV behaviour of this system. The differences between the solutions containing CTAB at concentrations lower and higher than the CMC seem to relate to the availability of more CTAB at the interface and possibly to the formation of multi-layered cathodic adsorbates [25]. The subtle details in the structure of the stripping peak are quantitatively affected by the CTAB concentration.

3.2 In situ surface-enhanced Raman spectroscopy

In situ SERS experiments were carried out during Cu ECP from the bath containing 2.5 mM CTAB. The experiments were run in the potentiostatic mode by shifting the cathodic potential in the range between OCP (+42 mV) and −1000 mV. This range comprises both the typical electrodeposition and the HER ranges. In the latter range metal plating may go on simultaneously with reactions of the organics, leading to special structural and chemical effects (see, e.g. [26]). The steady-state c.d. vs. potential relationship measured at a Cu electrode during SERS experiments is shown in Fig. 4 and exhibits essentially the same electrokinetic features as the voltammograms discussed in Sect. 3.1: (i) in the low overvoltage region, Cu ECP inhibited by adsorbed CTAB can be noticed, with a cathodic passivation peak (region A), (ii) followed by a

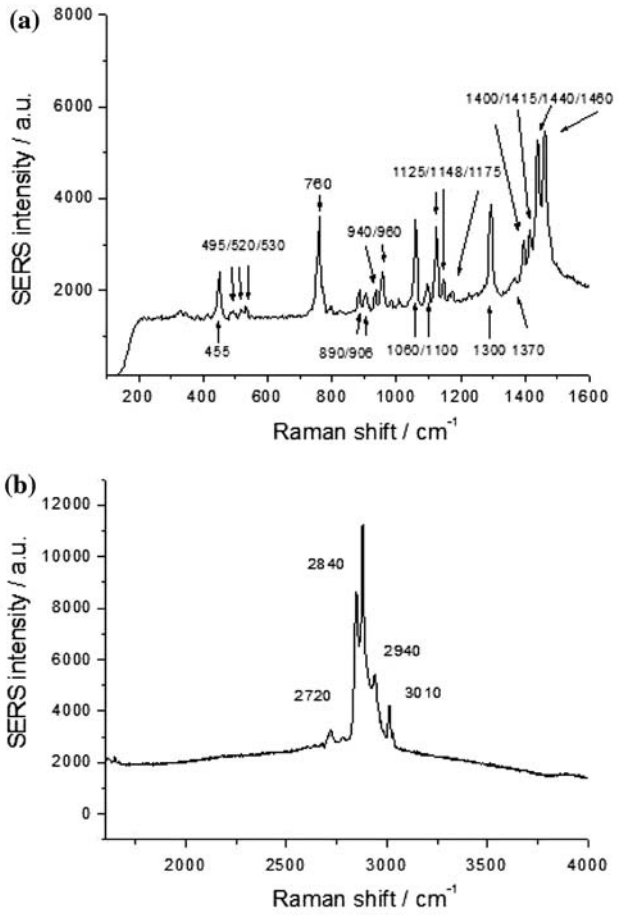

Fig. 5 Normal Raman spectrum of CTAB powder

Tafel region for Cu ECP (B) and (iii) corresponding mass-transport controlled regime (C), and (iv) eventually the high-potential Tafel region (D) where the hydrogen evolution reaction (HER) dominates. Cathodic passivation is a decrease of cathodic current density related to the adsorption of ligands released during the ECP process itself (for details, see e.g. [27]). The potential sampling was performed in steps of 10 mV for polarisation lower than −100 mV and of 50 mV for more cathodic conditions. Spectra were also measured at the same potentials in the reverse direction (from anodic to cathodic), but no appreciable changes could be detected and no further mention is made of these experiments. At −1000 mV a strong fluorescent bands appears, centred at ca. 3000 cm^{-1}, which does not allow measurement of spectra at more cathodic potentials.

For comparison, a normal Raman spectrum of CTAB powder was also recorded (Fig. 5a and b). The bands appearing in this figure are listed and assigned in the first column of Table 1. All the bands can be interpreted in terms of CTAB molecular and condensed-state vibrations. A selection of spectra measured during ECP and exhibiting typical spectral changes observed, are shown in Figs. 6–9. The leading spectral features are still those related to CTAB; they have been listed in Table 1 and will not be discussed further. Of course the bands observed with CTAB powder at 495, 520 and 530 cm^{-1}, corresponding to ammonium condensed-state bands [29], cannot be found in the SERS spectra recorded during ECP.

In addition to the CTAB features, some differences emerge, that can be explained in terms of adsorption and reaction; these changes have been reported and interpreted in the second and third columns of Table 1, respectively.

Table 1 Raman bands related to CTAB and its reaction products, observed with powder and during Cu electrodeposition experiments

Normal Raman powder	SERS during ECP	Band assignment	References
–	256[a]	Cu–N stretching	[28]
–	415[a]	Cu–N–C bending	[28]
455	450/460[a]	QA torsional oscillation	[29, p. 343]
495/520/530	–	QA condensed-state bands	[29, p. 393]
–	530/590 vw grows with cathodic polarisation	C–Cl stretching	[29, p. 393]
–	730 grows with cathodic polarisation	C–Cl stretching	[29] p. 393]
760	760[a]	CH_2 in phase rock	[29, p. 231]
890/906	905[a]	C–$N(CH_3)_3^+$ symm. stretching	[29, p. 344]
940/960/965	970[a]	C–$N(CH_3)_3^+$ asymm. stretching (asym?)	[29, p. 344]
1015 vw	1008[a] grows in (−45/− 150 mV)	in-phase C–C	[29, p. 225]
1060	1058[a] grows with cathodic polarisation	C–N stretching in aliphatic QA salt an amines	[29, p. 341]
1100/1125	1140 w[a]	C–C modes	[29, pp.228–230]
1148/1175			
1300 s/1370 w	1300 w[a] grows up to −350 mV, then decreases	CH_2 wagging	[29, p. 392]
1400	1415 vw[a]	CH_2 scissoring deformation	[29, p. 227]
1415			
1440/1460	1440, 1450[a]	C–$N(CH_3)_3^+$	[29, p. 344]
–	1570 (+42/− 80 mV)	Cl–CH = CHR stretching	[29, p. 251]
–	2200 (+42/− 150 mV)	NH^+ stretching & overtones/combination	[29, p. 344]
2720	2720–2730[a]	QA combination band	[29, pp. 343, 344]
2840/2880	2850[a]	CH_2/CH_3 symmetric stretching	[29, p. 227]
2940	2930[a]	CH_2 asymmetric stretching	[29, p. 227]
2970 sh	2965–2975[a]	CH_3 asymmetric stretching	[29, p. 219]
3010	3030[a]	Cl–CH_2 symmetric stretching of TM-QAS	[29, p. 344]
–	3500 (−350/− 900 mV)	N–H stretching	[29, p. 388]

Legenda- QA: quaternary ammonium; s: strong; sh: shoulder, vw: very weak; w: weak

[a] Peak visible at all the potentials, in the investigated range; if the relevant band is observed only in a potential range, this is given in brackets

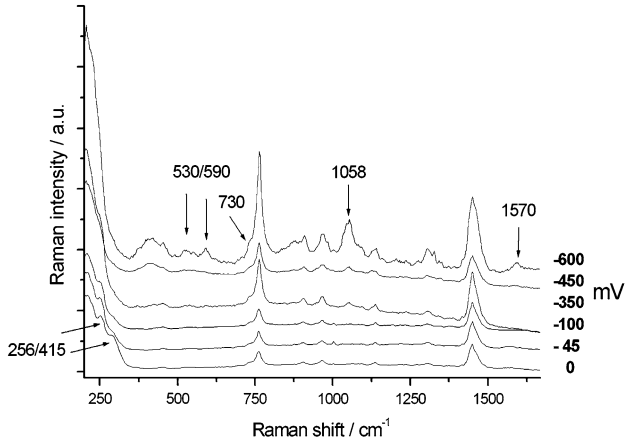

Fig. 6 In situ potential-dependent (0 to −0.6 V) SERS spectra recorded at a Cu electrode in contact with the Cu ECP bath containing 2.5 mM CTAB

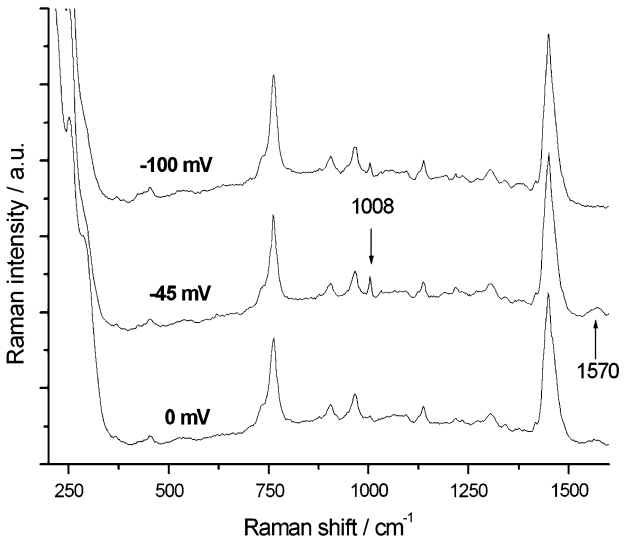

Fig. 7 In situ potential-dependent (0 to −0.1 V) SERS spectra recorded at a Cu electrode in contact with the Cu ECP bath containing 2.5 mM CTAB

In particular the following features are seen:

(i) extramolecular bands at 256 and 415 cm^{-1}, corresponding to Cu–N stretching and Cu–N–C bending modes, respectively (see Fig. 6) and deriving from the adsorption bond;

(ii) peaks at 530, 590 and 730 cm^{-1}, whose intensity correlates positively with cathodic polarisation (see Fig. 6), that can be explained by C–Cl stretching, this moiety forms in a cathodic reaction described below in this section;

(iii) a peak corresponding to the SERS band at 1008 cm^{-1} (in-phase C–C mode) is found in the normal Raman spectrum of CTAB powder at 1015 cm^{-1}. Nevertheless, the intensity of this peak grows progressively on shifting the potential from −45 to −150 mV—i.e. in the potential region where ECP goes on in the Butler-Volmer regime—and it decreases at higher cathodic potentials—where the ECP rate is controlled by mass-transport (see Fig. 7). The reason for this is that in the range −45 to −150 mV the surface coverage with the intact cationic surfactant tends to increase for electrostatic reasons, cathodic reactivity—leading to the detachment of the aliphatic tail (see below in this section)—correlates to a decrease in intensity of this chain mode at higher cathodic polarisation;

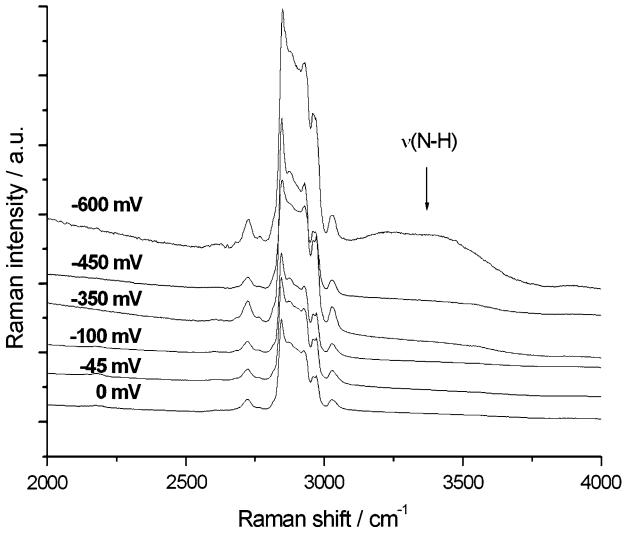

Fig. 8 In situ potential-dependent (0 to −0.6 V) SERS spectra recorded at a Cu electrode in contact with the Cu ECP bath containing 2.5 mM CTAB

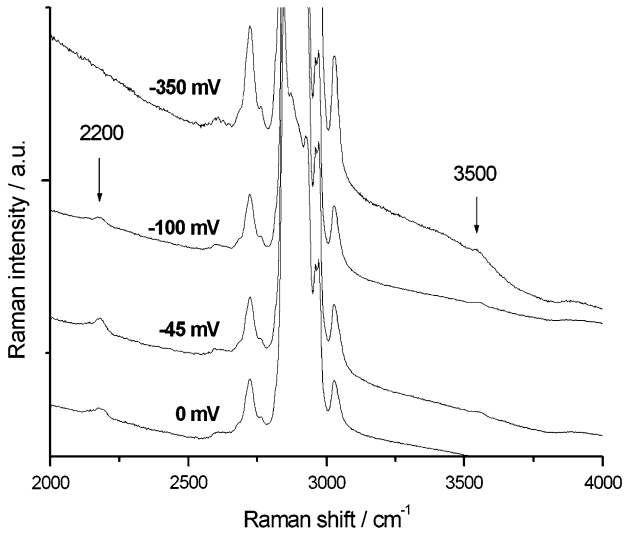

Fig. 9 In situ potential-dependent (0 to −0.1 V) SERS spectra recorded at a Cu electrode in contact with the Cu ECP bath containing 2.5 mM CTAB

(iv) again, the SERS peak at 1058 cm^{-1} corresponds to that at 1060 cm^{-1} (C–N stretching in aliphatic quaternary ammonium cation and amine) in the powder spectrum, but its intensity increases steadily with cathodic polarization, where mass-trasport controlled Cu ECP goes on in the presence of hydrogen evolution (see Figs. 6 and 7). This band corresponds to any tri-methyl quaternary ammonium cation [29], and its intensity is dominated by the progressive adsorption of reacted ammonium (with hydrogen substituting the aliphatic tail) and by the adsorption of cathodically formed amine (see below for a tentative reaction scheme).

(v) a new peak at 1570 cm^{-1} is found to develop on polarising the electrode cathodically (see Figs. 6 and 7), even though it is not found in some cases at intermediate cathodic potentials, probably for some subtle kinetic reasons, related to the interaction of adsorption and Cu discharge. This SERS band can be assigned to Cl–CH = CHR stretching, corresponding to the allylic reaction product postulated below;

(vi) a new peak at 2200 cm^{-1} can be found for cathodic potentials lower than −150 mV, where mass-transport starts to control Cu ECP (see Fig. 9). This band can be assigned to NH^+ stretching combined with overtones, this moiety corresponds to a cathodic reaction intermediate in the reaction scheme proposed below;

(vii) a band at ca. 3500 cm^{-1} is found in the range −350 to −900 mV; at the highest cathodic potentials studied this band becomes broad and unstructured. This vibration is typical of N–H stretching, corresponding to an hydrogenation product, described below.

CTAB adsorbed via the quaternary ammonium moiety, in the presence of Cl^- and H^+, seems to undergo the following reactions (I) and (II), described in [30]:

$$\left[(CH_3)_3{-}N-CH_2-(CH_2)_{10}{-}CH_3\right]^+_{ads} \xrightarrow[(I)]{Cl^-} N(CH_3)_{3ads} + Cl - CH_2 - (CH_2)_{10}{-}CH_3$$

$$N(CH_3)_{3ads} \xrightarrow[(II)]{+H^+} \left[N(CH_3)_3H\right]^+$$

At higher cathodic polarisation—within the HER range—coadsorbed H° is known to be able to induce hydrogenation reactions of coadsorbed organics (see [26] and references therein), in the present case, a mechanism, coherent with our spectral evidence, is reaction (III)

$$Cl - CH_2 - (CH_2)_{10}{-}CH_3 \xrightarrow[(III)]{+H^\circ} Cl - CH = CH - (CH_2)_9{-}CH_3 + H_{2(g)}$$

3.3 Characterisations by SEM and TEM

SEM observations were performed on electrodeposits obtained at −100 mV for 30 min (Fig. 10a), at −400 mV for 30 min (Fig. 10b) and at −700 mV for 30 min (Fig. 10c). These electrodeposition conditions correspond respectively to the potential interval A, to the Cu Tafel region B and to the Tafel region D reported in Fig. 4.

SEM observations show that for potentials lower than those required for mass-transport controlled Cu ECP (ca. −450 mV), we obtained compact layers with

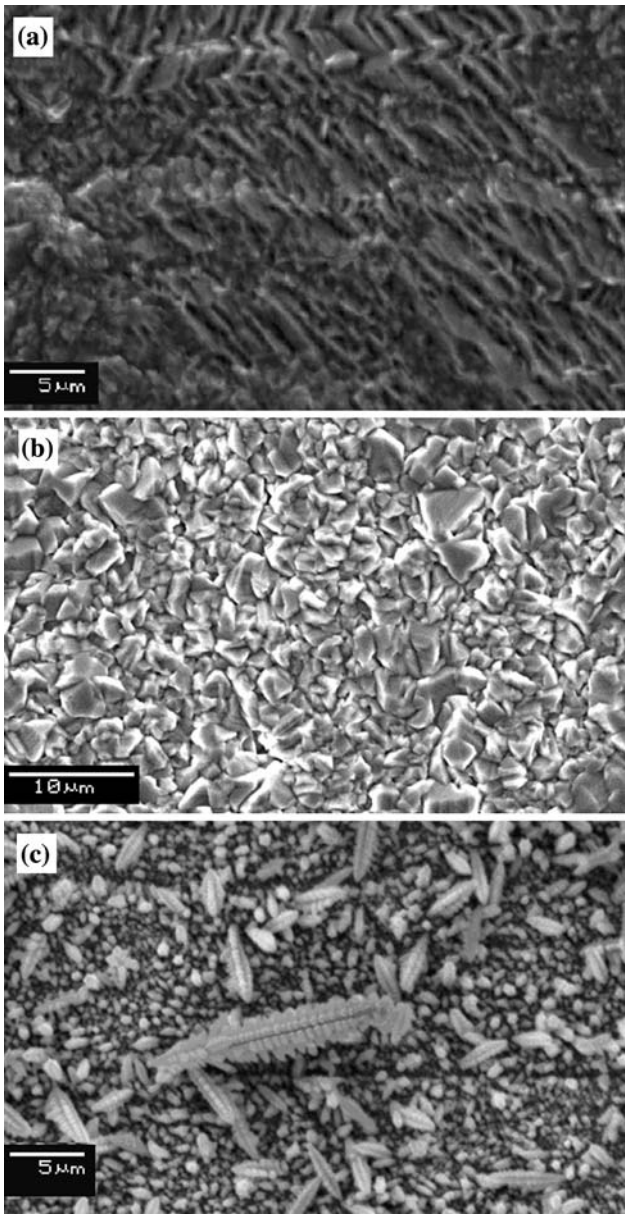

Fig. 10 SEM micrograph of a Cu electrodeposit obtained from the CTAB-containing bath at: (**a**) −100 mV, 30 min; (**b**) −400 mV, 30 min;. (**c**) −700 mV, 30 min

morphological differences between the CTAB-inhibition region (Fig. 10a) and the Cu Tafel region (Fig. 10b). In the former case, ordered ridges are noticed, ca. 500 nm wide and extending between 5 and 10 μm in length; in the latter image, micrometric crystalline grains without an apparent preferred elongation tend to form. Within the HER range some evidence of dendrite growth is found (Fig. 10c).

TEM was useful to characterise some samples produced by operating within the HER range. In this range, in fact, the CTAB-containing bath meets the requirements for the formation of nanoparticles in the solution close to the cathode, where the particles can experience a potential gradient enabling them to work as bipolar beads in a fluidised bed in such a way as to ensure overall cathodic growth, as detailed in [31]. At lower cathodic polarisations, just above the limiting c.d. for Cu ECP, monodomain nanoparticles of dimensions ca. 5 nm tend to grow (see BF TEM images in Fig. 11a and the correlated HRTEM image in Fig. 11b), nanoparticles grown at −700 mV, 30 min of electrolysis. At higher cathodic potentials, multidomain nanoparticles ca. 20 nm in diameter are found (see BF TEM and HRTEM images in Fig. 11c and d), respectively: nanoparticles grown at −1000 mV, 30 min of electrolysis).

An explanation of this potential effect might be that the enhanced de-composition rate of the surfactant under higher cathodic polarisations impacts the stability of nanoparticles thus favouring their agglomeration. In fact, the detachment of the aliphatic tail from the ammonium moiety gives rise to fact that the species adsorbed at the Cu nanoparticles impart to them a lower degree of mutual isolation.

4 Conclusions

On the basis of cyclic voltammtery, surface enhance Raman spectroscopy as well as SEM and TEM characterisations, we assessed the effects of CTAB and its

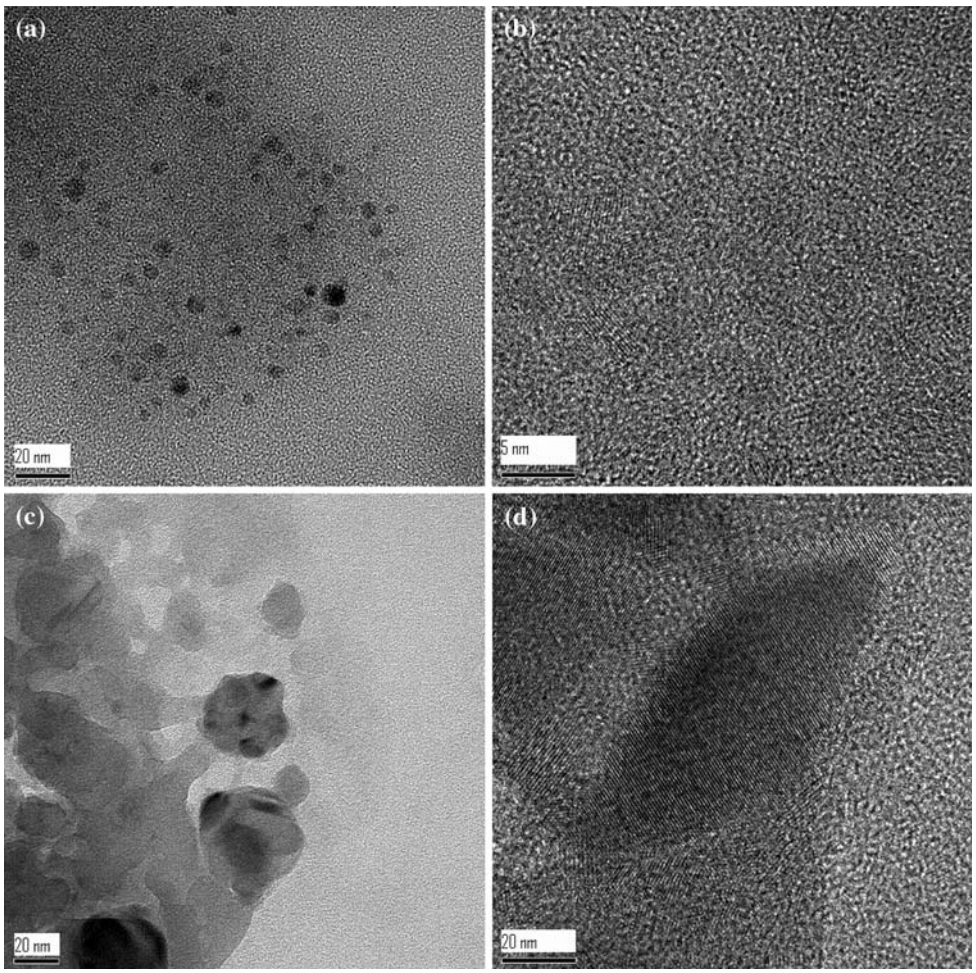

Fig. 11 (**a**) A typical TEM BF image of nanoparticles grown at −700 mV, 30 min of electrolysis. (**b**) A High-Resolution TEM (HRTEM) image of some particles in (**a**). (**c**) A TEM BF image of nanoparticles grown at −1000 mV, 30 min of electrolysis. (**d**) The High-Resolution TEM (HRTEM) image of a small area of the sample in (**c**)

cathodic reactivity on Cu ECP and, in particular, on the structure of electrodeposited Cu.

In situ SERS experiments carried out during the electrodeposition of Cu disclosed that CTAB and its cathodic reaction products are adsorbed at the cathode in a wide potential range, from very low cathodic polarisations up to the hydrogen-evolution range. Removal of the aliphatic tail, occurring via nucleophilic attack by chlorides, prevails at cathodic voltages below the HER threshold, while hydrogenation of the chlorinated product takes places via hydrogen radicals produced in the HER range.

CTAB gives rise to inhibition of the ECP process, including cathodic passivation at low electrodeposition overvoltages. Under highly inhibited ECP conditions, compact deposits with ordered ridges tend to form. At cathodic potentials exceeding the inihibition range, but low enough to corresponding to c.d.s well below the limiting c.d. for Cu^{2+} reduction, compact grainy films are produced. Under mass-transport control, dendritic and loose Cu grows at the cathode and nanoparticles tend to form in the solution layer facing the cathode. The sizes of the Cu nanoparticles are positively correlated with the cathodic overvoltage, owing to progressively increasing rate of the cathodic QAS decomposition and attending decrease of the colloid-protecting properties of the additive.

References

1. Franklin TC (1986) J Electrochem Soc 133:893
2. Franklin TC (1988) J Electrochem Soc 135:1638
3. Schweinsberg DP, Ashworth V (1988) Corr Sci 28:539
4. Cachet C, Wiart R, Ivanov I, Stefanov Y, Rashkov S (1994) J Appl Electrochem 24:713
5. Zvauya R, Dawson JL (1994) J Appl Electrochem 24:943
6. Muralidharan S, Iyer SVK, Vasudevan T, Alwarappan S (1995) Corr Sci 37:1235
7. Tripathy BC, Das SC, Hefter GT, Singh P (1998) J Appl Electrochem 28:915
8. Narayanan TSNS (1999) Metal Finishing 6:94
9. Bozzini B, Fanigliulo A, Serra M (2001) J Cryst Growth 231:589
10. Bizzotto D, Zamlynny V, Burgess I, Jeffrey CA, Li HQ, Rudinstein J, Merril RA, Lipkowski J, Galus Z, Nelson A, Pettinger B (1999) In: Wieckowski A (ed) Interfacial electrochemistry–theory, experiment, applications. Marcel Dekker, New York
11. Bartlett PN (2004) Interface 13:28
12. Reetz MT, Helbig W (1994) J Am Chem Soc 116:7401
13. Becker JA, Schäfer R, Festag W (1995) J Chem Phys 103:2520
14. Reetz MT, Helbig W, Quaiser SA (1995) Chem Mater 7:2227
15. Reetz MT, Quaiser SA (1995) Angew Chem Int Ed Engl 34:2240
16. Kolb U, Quaiser SA, Winter M, Reetz MT (1996) Chem Mater 8:1889
17. Reetz MT, Helbig W, Quaiser SA (1996) In: Fürstner A (ed) Active metals. VCH, Weinheim
18. Reetz MT, Quaiser SA, Merk C (1996) Chem Ber 129:741
19. Kang KH, Kim HU, Lim KH (2001) Colloids Surf A 189:113
20. Bozzini B, D'Urzo L, Mele C (2007) Electrochim Acta 52:4767
21. Lee HP, Nobe K (1986) J Electrochem Soc 133:2035
22. Abrantes LM, Araùjo LM, Levi M (1995) Min Eng 8:1467
23. Drissi-Daoudi R, Irzho A, Darchen A (2003) J Appl Electrochem 33:339
24. Bozzini B, Busson B, De Gaudenzi GP, D'Urzo L, Mele C, Tadjeddine A (2007) Corr Sci 49:2392
25. Montalvo G, Valiente M, Rodenas E (1995) J Colloids Interface Sci 172:494
26. Bozzini B, Romanello V, Mele C, D'Urzo L (2008) J Phys Chem C 112:6352
27. Bozzini B, Giovannelli G, Cavallotti PL (1999) J Appl Electrochem 29:687
28. Bozzini B, Mele C, Fanigliulo A, Busson B, Vidal F, Tadjeddine A (2004) J Electroanal Chem 574:85
29. Colthup NB, Daly LH, Wiberley SE (1990) Introduction to infrared and Raman spectroscopy. Academic Press, Boston
30. Isaacs NS (1987) Physical organic chemistry. John Wiley & Sons, New York
31. Bozzini B, Romanello V, De Gaudenzi GP (2006) Trans Inst Met Fin 84:154